

# Spectral Signature of Alpine Snow Cover from the Landsat Thematic Mapper

*Jeff Dozier*

*Department of Geography and Center for Remote Sensing and Environmental Optics,  
University of California, Santa Barbara and  
Jet Propulsion Laboratory, California Institute of Technology*

**M**apping of snow and estimation of snow characteristics from satellite remote sensing data require that we distinguish snow from other surface cover and from clouds and compensate for the effects of the atmosphere and rugged terrain. The spectral signature of the snowpack is calculated from a radiative transfer model, accounting for scattering and absorption by the ice grains, water inclusions, and particulates. In interpreting the spectral reflectance measured from the Thematic Mapper, or from any other satellite, we need to account for topographic effects without requiring that satellite data be precisely registered to digital elevation data, because the poor quality of most digital elevation data introduces considerable noise into calculations of slope and azimuth. For a range of snow types, atmospheric profiles, and topographic illumination conditions, I estimate typical spectral signatures for the Landsat Thematic Mapper. TM images of the southern Sierra Nevada are analyzed to distinguish several classes of snow from other surface covers. Snow can be reliably

distinguished from other surfaces and from clouds at all sun angles encountered in the mid-latitudes. In TM Band 1 or 2, snow is brighter than other natural surfaces, and in Band 5 clouds are usually much more reflective than snow. Therefore, the intersection of the following criteria maps the snow cover: planetary reflectance  $R_p$  in TM Band 1 is greater than about 0.16;  $R_p(\text{TM5})$  is less than about 0.2; the normalized Band 2-5 difference,  $[R_p(\text{TM2}) - R_p(\text{TM5})] / [R_p(\text{TM2}) + R_p(\text{TM5})]$ , is greater than about 0.4. Large surface grain sizes can be distinguished from areas where the grain size is finer at the snow surface, using TM Bands 2, 4, and 5. Because of saturation in TM Band 1, estimation of the degree of contamination by absorbing aerosols is not feasible.

## INTRODUCTION

Water in its frozen states accounts for more than 80% of the total fresh water on Earth and is the largest contributor to rivers and ground water over major portions of the middle and high latitudes. Snow and ice also play important interactive roles in the Earth's radiation balance, because snow has a higher albedo than any other natural surface.

Address correspondence to Jeff Dozier, CSL/CRSEO, Univ. of California, Santa Barbara, CA 93016

Received 25 August 1988; revised 16 February 1989.

Over 30% of the Earth's land surface is seasonally covered by snow, and 10% is permanently covered by glaciers. Snow cover represents a changing atmospheric output resulting from variability in the Earth's climate, and it is also a changing boundary condition in climate models. Thus, understanding of global and regional climates and assessment of water resources require that we monitor the temporal and spatial variability of the snow cover over land areas, from the scale of small drainage basins to continents.

The alpine snow cover and alpine glaciers in the mid-latitudes are important in both the climatic and hydrologic contexts—to examination of global and regional climates and to use of water resources (Colbeck et al., 1979; Walsh, 1984). Much of the uncertainty and sensitivity in the global hydrologic cycle lies in these reservoirs of frozen water, and the melting of alpine glaciers during the last half-century appears to account for much of the corresponding rise in sea level (Meier, 1984).

Over the last two decades satellite remote sensing has opened the possibility of data acquisition at regular intervals, and operational as well as research-oriented satellites have provided information on snow cover. Remote sensing of the seasonal snow cover has been used to improve the monitoring of existing conditions and has been incorporated into several runoff forecasting and management systems. Satellite sensors in the visible and near-infrared wavelengths provide information on the spatial distribution of parameters of hydrologic importance. From these reflectance measurements, we can measure snow-covered area, rates of snow-cover depletion, and surface albedo. The Landsat systems, in particular, are a source of data for hydrological and glaciological research at the scale of drainage basins.

The most common use of remote sensing in snow studies is to monitor snow-covered area (Rango and Itten, 1976; Rango et al., 1977). These efforts have been carried one step further by including satellite-derived measurements of snow-covered area as an index in a snowmelt runoff model (Rango and Martinec, 1979). The next step is to use satellite radiometric data to measure snow water equivalence and snow surface properties that are necessary for the calculation of the surface energy balance (Dozier et al., 1981b). While mea-

surements of snow water equivalence require data in the active or passive microwave region of the spectrum, mapping of snow cover and estimate of surface reflectance require data in the visible and near-infrared region. Identification of snow in level areas during daylight hours is straightforward during clear weather, because of high albedo of snow in the visible wavelengths. Automatic discrimination between snow and clouds is possible with a wavelength band between 1.55 and 1.75  $\mu\text{m}$ , where clouds are brighter than snow (Valovcin, 1976; Crane and Anderson, 1984; Dozier, 1984).

However, in rugged terrain, snow in the shadows can be darker than soil or vegetation in the sunlight, so that snow mapping in the mountains is not so easily accomplished. In alpine areas, therefore, the problems of correct interpretation of the satellite signal are severe. Because of the paucity of adequate digital elevation data, both in the United States and world-wide, the multispectral signal must usually be interpreted without knowledge of local illumination angles. Satellite data at a similar spatial scale to that of the topographic relief, i.e., a few tens of meters, are available, either from the Landsat Thematic Mapper (TM) or from the French Systeme Probatoire d'Observation de la Terre (SPOT). The TM has the better spectral coverage, whereas SPOT has a finer spatial resolution and pointing capability. In either case, the extremely large data volume makes the analysis difficult. How we use such data to measure key areas of the alpine snow and ice cover is a challenging issue. Therefore we seek procedures for the analysis which are as automated as possible.

## **RADIOMETRIC CHARACTERISTICS OF THE THEMATIC MAPPER**

The radiometric characteristics of the Landsat Thematic Mapper are summarized elsewhere in this issue of *Remote Sensing of Environment* (Barker and Wanchoo, 1989). In this section the same information is presented in a form more easily interpreted for analysis of bright surfaces such as snow.

All my calculations of the spectral signature of snow of various properties and under various atmospheric and topographic conditions use as the

Table 1. Landsat-5 TM Radiometric Characteristics

Band	Wavelength Range ( $\mu\text{m}$ )		Satellite Radiances ( $\text{Wm}^{-2} \mu\text{m}^{-1} \text{sr}^{-1}$ )		Exoatmospheric Solar Irradiance ( $\text{Wm}^{-2} \mu\text{m}^{-1}$ )
			$L_{\min}$	$L_{\max}$	$S_0$
TM1	0.45	0.52	-1.5	152.1	1957
TM2	0.53	0.61	-2.8	296.8	1829
TM3	0.62	0.69	-1.2	204.3	1557
TM4	0.78	0.90	-1.5	206.2	1047
TM5	1.57	1.78	-0.37	27.19	219.3
TM7	2.10	2.35	-0.15	14.38	74.52

Source: Data from Markham and Barker (1985; 1987).

fundamental physical quantity the “apparent planetary reflectance,” the apparent directional-hemispherical reflectance of the Earth-atmosphere system if the angular distribution of the reflected radiation is assumed to be isotropic. For each band represented by wavelength  $\lambda$ , therefore, the digital radiance numbers  $Q_{\text{cal}}$  on the satellite image are converted first to radiances  $L(\lambda)$  and then to planetary reflectances  $R_p(\lambda)$ :

$$L(\lambda) = L_{\min}(\lambda) + [L_{\max}(\lambda) - L_{\min}(\lambda)] \left( \frac{Q_{\text{cal}}}{Q_{\text{cal,max}}} \right) \quad (1)$$

$$R_p(\lambda) = \frac{\pi d^2 L(\lambda)}{\mu_0 S_0(\lambda)} \quad (2)$$

$\mu_0$  is the cosine of the solar illumination angle,  $d$  is the Earth-Sun radius vector, and  $S_0(\lambda)$  is the exoatmospheric solar irradiance in the same wavelength band. Either local slope or non-Lambertian reflectance can cause values of  $R_p$  to sometimes exceed 1.0.  $L_{\min}(\lambda)$  and  $L_{\max}(\lambda)$ , the radiances corresponding to  $Q_{\text{cal}} = 0$  and  $Q_{\text{cal,max}}$ , are given in Table 1 for Landsat-5 TM data processed after 15 January 1984. The minimum and maximum radi-

ances are the same for Landsat-4, but the wavelength ranges and, therefore, exoatmospheric radiances differ slightly (Markham and Barker, 1987).

Table 2 uses the data in Table 1 to calculate the quantization errors and maximum values of planetary reflectances at the approximate time of the Landsat overpass, for several dates at latitude  $37^\circ\text{N}$ , the middle latitude in the southern Sierra Nevada. The quantization error  $NE\Delta R_p$  is the change in planetary reflectance corresponding to a change of one digital radiance number, averaged over the range from the smallest positive radiance to the saturation radiance. The maximum reflectance corresponds to the saturation radiance. At this latitude, TM Band 1 will usually saturate over snow, except in the shadows, during all months. Plate I identifies saturated pixels in TM Bands 1, 2, and 4 for a typical image, and Figure 1 shows histograms of digital radiance numbers for three dates for these TM bands. TM1 frequently saturates. TM2 and TM3 will not usually saturate in December or January, will occasionally saturate in February, and will frequently saturate on slopes exposed to the Sun throughout the spring. TM4 will only occasionally saturate, after new snow in

Table 2. Quantization Error ( $NE\Delta R_p$ ) and Maximum Planetary Reflectance ( $R_{p,max}$ ) in TM Bands, at  $37^\circ\text{N}$  at Time of Landsat Overpass (about 10:00 Local Time)

Band	15 December		15 February		15 April		15 June	
	$NE\Delta R_p$	$R_{p,max}$						
TM1	0.0023	0.583	0.0018	0.463	0.0012	0.313	0.0011	0.289
TM2	0.0048	1.217	0.0038	0.966	0.0026	0.654	0.0024	0.603
TM3	0.0039	0.984	0.0031	0.781	0.0021	0.529	0.0019	0.487
TM4	0.0059	1.477	0.0047	1.173	0.0031	0.794	0.0029	0.732
TM5	0.0037	0.930	0.0029	0.738	0.0020	0.500	0.0018	0.461
TM7	0.0058	1.447	0.0046	1.149	0.0031	0.778	0.0029	0.717

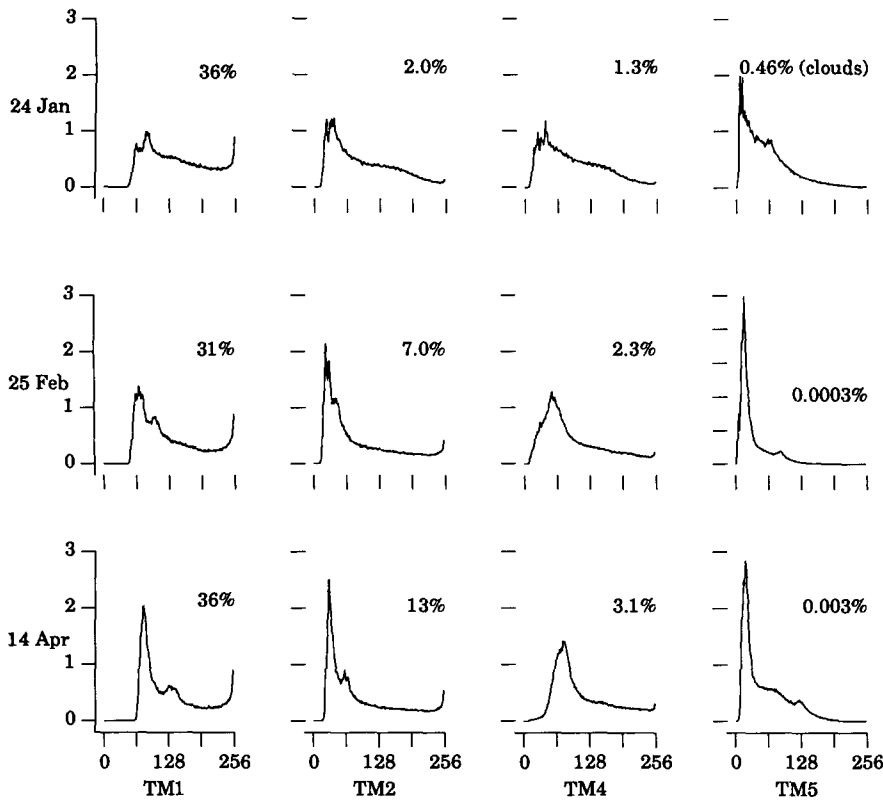


Figure 1. Histograms of digital radiance numbers for TM Bands 1, 2, 4, and 5 for three dates in the southern Sierra Nevada. Top: 24 January 1985. Middle: 25 February 1985. Bottom: 14 April 1985. Also shown are the percentages of saturated pixels in each band.

the spring, and TM5 and TM7 should never saturate over snow in the mid-latitudes, but may saturate over clouds or bright soils.

### SCATTERING AND ABSORPTION OF LIGHT BY SNOW AND ATMOSPHERE

The scattering and absorption of light by the snowpack, clouds, and the atmosphere are analyzed with a multiple-scattering model, a two-stream approximation to the radiative transfer equation. The fundamental scattering properties of the ice grains and water inclusions in the snowpack, the water droplets or ice crystals in clouds, and the aerosols in the atmosphere are calculated by the complex angular momentum approximation to the Mie equations (Nussenzveig and Wiscombe, 1980). The LOWTRAN model (Kneizys et al., 1988) is used to obtain values for molecular absorption in the atmosphere at the desired wavelengths.

The radiative transfer equation (Chandrasekhar, 1960) is used to calculate multiple scattering and absorption of the incident radiation. In our examination of the spectral properties of snow and clouds and the atmospheric effects in the TM bands, it is computationally time-consuming to calculate the angular distribution of the reflected radiation, but it is comparatively simple to examine the reflectance integrated over all angles. That is, we restrict discussion here to the spectral “directional-hemispherical” reflectance (Nicodemus et al., 1977), defined as the ratio of the reflected flux, the radiance (intensity) integrated over all angles, divided by the incoming direct irradiance:

$$R_s(\mu_0) = \frac{\int_0^{2\pi} \int_0^1 \mu L(\mu, \phi) d\mu d\phi}{\mu_0 F_0} = \frac{F_{\uparrow}}{\mu_0 F_0} \quad (3)$$

$L(\mu, \phi)$  is the radiance in the upward direction at angle  $\arccos \mu$ , azimuth  $\phi$ .  $F_0$  is the direct irradiance at the top of the medium, incident at angle  $\arccos \mu_0$ .

We can solve this kind of problem analytically with the two-stream approximation to the radiative

transfer equation for a homogeneous medium (Meador and Weaver, 1980):

$$\frac{dF_{\uparrow}(\tau)}{d\tau} = \gamma_1 F_{\uparrow}(\tau) - \gamma_2 F_{\downarrow}(\tau) - \gamma_3 \omega_0 F_0 e^{-\tau/\mu_0}, \quad (4a)$$

$$\frac{dF_{\downarrow}(\tau)}{d\tau} = \gamma_2 F_{\uparrow}(\tau) - \gamma_1 F_{\downarrow}(\tau) + \gamma_4 \omega_0 F_0 e^{-\tau/\mu_0}. \quad (4b)$$

$F_{\uparrow}$  and  $F_{\downarrow}$  are upward and downward fluxes,  $\omega_0$  is the single-scattering albedo (i.e., the ratio of extinction by scattering to total extinction), and the  $\gamma$  values parametrize the scattering phase function. The Mie equations are used to calculate the single-scattering albedo  $\omega_0$  and the scattering asymmetry parameter  $g$ , and the  $\gamma$  values are functions of  $\omega_0$ ,  $g$ , and  $\mu_0$ . To estimate the optical depth coordinate  $\tau$  as a function of physical properties, we also need the extinction efficiency  $Q_{\text{ext}}$  and the number density of the scatterers.

Top and bottom boundary conditions are needed for the solution of (4a), (4b). At the top of the medium we postulate no downward diffuse flux. At the bottom, optical depth  $\tau_0$ , the upward diffuse flux is the reflected diffuse and direct radiation from a horizontal surface, whose reflectance is  $R_0$ . Thus, the boundary conditions for a level surface are

$$F_{\downarrow}(0) = 0, \quad (5a)$$

$$F_{\uparrow}(\tau_0) = R_0 [F_{\downarrow}(\tau_0) + \mu_0 F_0 e^{-\tau_0/\mu_0}] \quad (5b)$$

With these boundary conditions, the two-stream equations can be solved, and the values of  $F_{\downarrow}$  or  $F_{\uparrow}$  can be calculated for any level, within the atmosphere or the snowpack. A later section considers the modification of the lower boundary condition for rough topography.

The directional-hemispherical reflectance at the top of the medium is

$$R_s \equiv \frac{F_{\uparrow}(0)}{\mu_0 F_0} = \frac{1}{P^+ V^- - P^- V^+} \times \left[ \omega_0 (Q^+ - Q^-) + 2\xi \gamma_2 e^{-\tau_0/\mu_0} \{ R_0 - q [\mu_0 (\alpha_1 R_0 - \alpha_2) + \gamma_4 R_0 + \gamma_3] \} \right] \quad (6)$$

and the directional-hemispherical transmittance  $T_s$  is

$$T_s \equiv \frac{F_{\downarrow}(\tau_0) + \mu_0 F_0 e^{-\tau_0/\mu_0}}{\mu_0 F_0} = \frac{2q\xi\gamma_2(\mu_0\alpha_1 + \gamma_4) + e^{-\tau_0/\mu_0}(P^+U^- - P^-U^+)}{P^+V^- - P^-V^+}, \quad (7)$$

where

$$P^{\pm} = (\gamma_1 \pm \xi) e^{\pm \xi \tau_0},$$

$$q = \frac{\omega_0}{1 - \xi^2 \mu_0^2},$$

$$Q^{\pm} = \frac{V^{\mp} e^{\pm \xi \tau_0} (\alpha_2 \pm \xi \gamma_3)}{1 \pm \xi \mu_0},$$

$$U^{\pm} = \gamma_2 - \frac{\omega_0 (\alpha_2 \pm \xi \gamma_3)}{1 \pm \xi \mu_0},$$

$$V^{\pm} = \gamma_2 - R_0 (\gamma_1 \pm \xi),$$

$$\xi^2 = \gamma_1^2 - \gamma_2^2,$$

$$\alpha_1 = \gamma_1 \gamma_4 + \gamma_2 \gamma_3,$$

$$\alpha_2 = \gamma_2 \gamma_4 + \gamma_1 \gamma_3.$$

Meador and Weaver (1980, Table 1) give  $\gamma$  expressions for seven different two-stream approximations, as functions of  $\mu_0$ ,  $\omega_0$ , and the scattering asymmetry parameter  $g$ . For the calculations in this paper I used the Meador-Weaver hybrid method.

For deep snowpacks, "semi-infinite," the underlying surface has no effect. Letting  $\tau_0 \rightarrow \infty$  in Eq. (6) leads to

$$R_s^{(\infty)} = \frac{\omega_0 [\gamma_3 (\xi + \gamma_1 - \gamma_2) + \gamma_2]}{(\xi + \gamma_1)(1 + \xi \mu_0)}. \quad (8)$$

## OPTICAL PROPERTIES OF SNOW AND CLOUDS IN TM BANDS

Snow is a collection of ice grains and air, and, when at 0°C, it also has a significant fraction of liquid water. Snow also often includes particulate and chemical impurities—dust, soot, pollen and other plant material—and small amounts of the major cations and anions. Thus the optical properties of snow depend on the bulk optical properties and the geometry of the ice grains, the liquid

water inclusions, and the solid and soluble impurities. Similarly, clouds are composed of water droplets, sometimes ice crystals, and they may contain impurities.

### Bulk Optical Properties of Ice and Water

In the visible and near-infrared wavelengths the bulk optical properties of ice and water are very similar, so that the reflectance and transmittance of the snowpack in this region of the electromagnetic spectrum depend on the wavelength variation of the refractive index of ice, the grain size distribution of the snow, the depth and density of the snowpack, and the size and amount of those impurities whose refractive indices are substantially different from those of ice and water. The reflectance of wet snow in the near-infrared is lower than that of dry snow, but mainly because of microstructural changes caused by the water, except in some narrow spectral regions where the optical properties of water are different than those of ice. Similarly, the reflectance and transmittance of clouds depend on the geometric thickness, the number density of the droplets, and their size distribution.

The most important optical property of ice and water, which causes spectral variation in the reflectance of snow and clouds in visible and near-infrared wavelengths, is that the absorption coefficient (i.e., the imaginary part of the refractive index) varies by 7 orders of magnitude in the wavelengths from 0.4 to 2.5  $\mu\text{m}$ . Figure 2 shows the complex refractive index  $n + ik$  for ice and water. The important properties to note are

1. The spectral variation in the real part  $n$  is small, and the difference between ice and water is not significant.
2. The absorption coefficients  $k$  of ice and water are very similar, except for the region between 1.55 and 1.75  $\mu\text{m}$ , where ice is slightly more absorptive.
3. In the visible wavelengths both ice and water are highly transparent so  $k$  is small.
4. In the near-infrared wavelengths ice and water are moderately absorptive, and the absorption increases with wavelength.

The bottom part of Fig. 2 shows the absorption in a slightly different manner. Transmission of

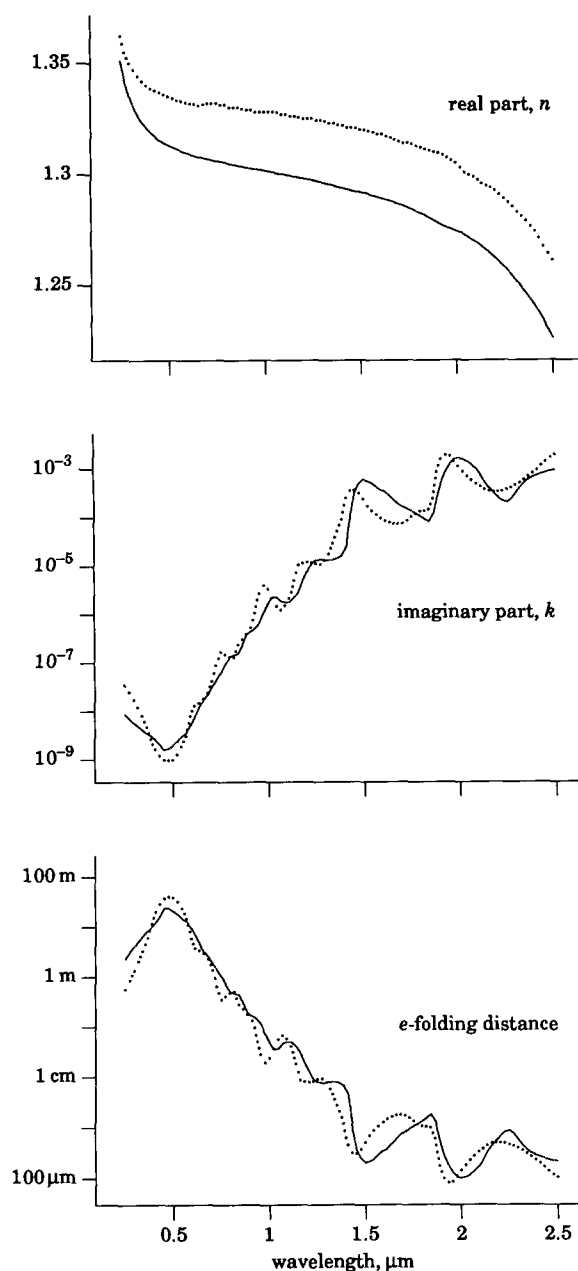


Figure 2. Complex refractive index ( $n + ik$ ) and  $e$ -folding distance of ice (Warren, 1984) (—) and water (Hale and Querry, 1973; Palmer and Williams, 1974; Downing and Williams, 1975) (···). Upper: real part of refractive index ( $n$ ). Middle: imaginary part of refractive index ( $k$ ). Lower:  $e$ -folding distance, at which intensity is reduced to  $e^{-1}$ .

light along distance  $s$  through a pure substance decays as  $e^{-4\pi ks/\lambda}$ . The bottom graph shows the spectral variation of  $\lambda/4\pi k$ , the “ $e$ -folding distance,” i.e., the distance through which light will propagate through pure ice or water before its intensity is reduced to  $e^{-1}$  times its initial value.

### Spectral Reflectance of Snow in the TM Bands

The spectral and angular variation in snow reflectance are modeled by the radiative transfer equation, as shown to be appropriate by Bohren and Barkstrom (1974) and Warren (1982). The model used for these calculations was presented in a previous section on Scattering and Absorption of Light. In the visible wavelengths ice is highly transparent, so that the albedo of snow is sensitive to small amounts of absorbing impurities (Warren and Wiscombe, 1980). In the near-infrared wavelengths ice is more absorptive, so the albedo depends primarily on grain size (Wiscombe and Warren, 1980). We make the following assumptions in modeling the reflectance of snow. Most of these assumptions have yet to be tested by rigorous measurements of physical properties and spectral reflectance of the same snowpack, but the model produces reflectance spectra that match those of snow (Warren, 1982).

1. The reflectance of snow is modeled as a multiple scattering problem. Scattering properties of irregularly shaped grains are mimicked by Mie calculations for an "equivalent sphere," for which the best candidate in the wavelength region from 0.4 to 1.1  $\mu\text{m}$  is apparently the sphere with the same surface-to-volume ratio (Dozier et al., 1988), which can be measured by stereological methods applied to snow samples (Davis and Dozier, 1989). Although snow grains are irregularly shaped, they are usually not oriented, so that the assumption that their scattering properties can be mimicked by some spherical radius  $r$  is reasonable, especially when we want to describe the general spectral properties. When we want details about the angular characteristics of the reflectance, the spherical assumption could become more critical.
2. Near-field effects are assumed unimportant. The fact that the ice grains in a snowpack touch each other apparently does not affect the snow's reflectance, because the center-to-center spacing is still much larger than the wavelength. That is, snow reflectance is independent of density up to about  $650 \text{ kg m}^{-3}$ . Reflectance measurements carried out under field conditions over a season and simply analyzed statistically *will* show a significant in-

verse relationship between density and reflectance, but the physical model shows that the explanation for changes in reflectance lies in other properties of the snow cover, namely an increase in grain size and in the amount of contaminants near the surface.

3. The effect of absorbing impurities (dust, soot) can be modeled either as separate spheres (smallest effect) or as concentric spheres with the impurity in the center (largest effect). These should bound the magnitude.

The total optical depth of a snowpack,  $\tau_0$ , is a function of the extinction efficiency  $Q_{\text{ext}}$  and the snow water equivalence  $W$  (mass per unit area), which is the product of mean snow density  $\rho_{\text{snow}}$  and depth  $h$ . Therefore the value for the optical depth of snow used in the radiative transfer model [Eqs. (6) and (7)] is

$$\tau_0 = \frac{3WQ_{\text{ext}}}{4r\rho_{\text{ice}}} = \frac{3\rho_{\text{snow}}hQ_{\text{ext}}}{4r\rho_{\text{ice}}}. \quad (9)$$

Figure 3 shows the spectral reflectance  $R_s^{(\infty)}$  of pure, deep snow [i.e., using Eq. (8)], for snow grain radii from 50 to 1000  $\mu\text{m}$  (0.05 to 1.0 mm), representing a range from new snow to spring snow, although the grain clusters in coarse spring snow can exceed 5 mm in radius. Because ice is so transparent in the visible wavelengths, increasing the grain size does not appreciably affect the reflectance. The probability that a photon will be absorbed, once it enters an ice grain, is small, and that probability is not increased very much if the ice grain is larger. In the near-infrared, however, ice is moderately absorptive. Therefore, the reflectance is sensitive to grain size, and the sensitivity is greatest at wavelengths from 1.0 to 1.3  $\mu\text{m}$ . Because the ice grains are strongly forward-scattering in the near-infrared, reflectance increases with illumination angle, especially for larger grains, as shown in Figure 3.

Because the complex indices of refraction of ice and water are similar, liquid water *per se* has little effect on the reflectance of snow. Except where meltwater ponds in depressions when melting snow overlies an impermeable substrate, or when rain falls on fine-grained snow, liquid water content in snow rarely exceeds 5 or 6%. This small amount of water does not affect the bulk radiative transfer properties, except possibly in a few narrow wavelength regions where the absorption co-

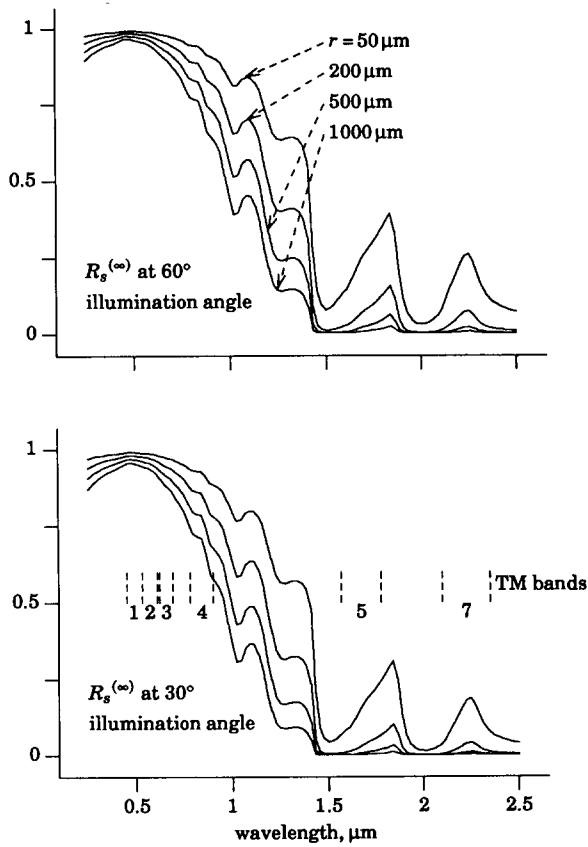


Figure 3. Directional-hemispherical reflectance  $R_s^{(\infty)}$  of deep snow at illumination angles 60° and 30°, for wavelengths from 0.4 to 2.5  $\mu\text{m}$ . The curves represent grain radii of 50  $\mu\text{m}$  (upper), 200  $\mu\text{m}$ , 500  $\mu\text{m}$ , and 1000  $\mu\text{m}$  (lower). In the visible wavelengths (0.4–0.7  $\mu\text{m}$ ) reflectance is insensitive to grain size. In the near-infrared, especially from 0.9 to 1.3  $\mu\text{m}$ , reflectance is very sensitive to grain size. From 1.55 to 1.7  $\mu\text{m}$  reflectance is sensitive, but only for small sizes. The effect of illumination angle is greatest in the near-infrared.

efficients are appreciably different (Hyvärinen and Lammasniemi, 1987). Instead, the decreases in reflectance that occur as snow melts result from the effective size increase caused by the two- to four-grain clusters that form in wet, unsaturated snow (Colbeck, 1979; 1986). These apparently behave optically as single grains.

Although the reflectance in the visible wavelengths is insensitive to grain size, it is affected by two variables, finite depth, and the presence of absorbing impurities. Figure 4 shows spectral reflectance for a range of grain sizes of snow water equivalences from 10 to 100 mm, over a black surface. For large grains,  $r = 1$  mm, reflectance of snow with a water equivalence of as large as 100

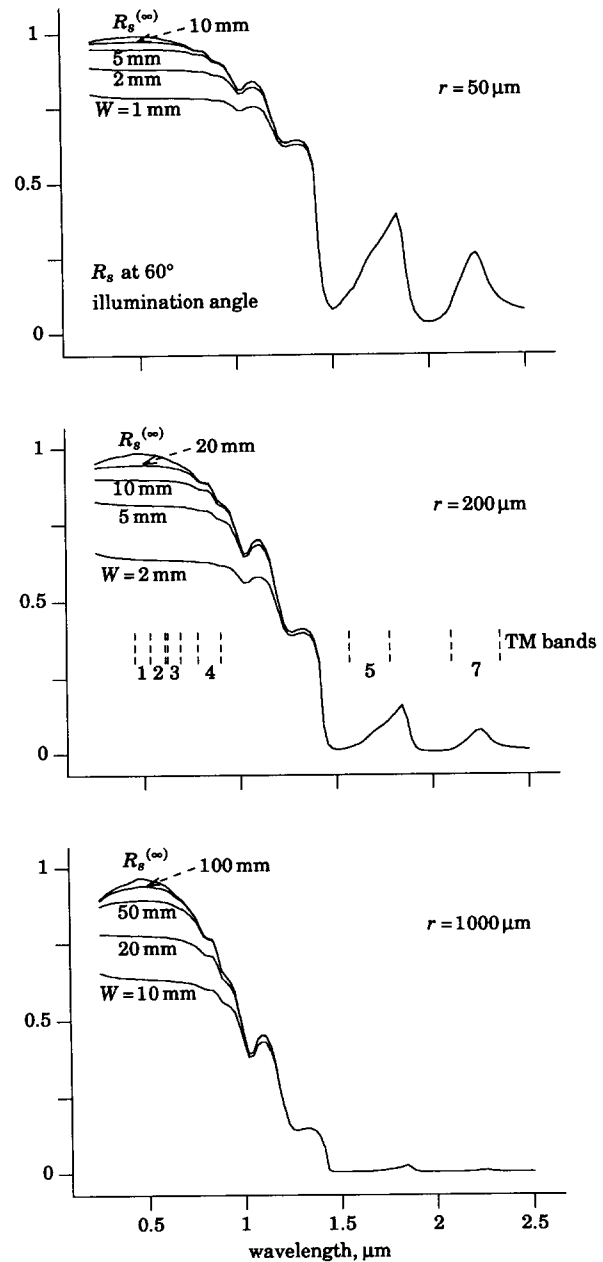


Figure 4. Directional-hemispherical reflectance  $R_s$  of finite-depth snow at illumination angle 60°, for wavelengths from 0.4 to 1.5  $\mu\text{m}$ , and grain radii  $r = 50 \mu\text{m}$ , 200  $\mu\text{m}$ , and 1000  $\mu\text{m}$ . For large grain sizes, a change in reflectance in the visible wavelengths is perceptible when the snow water equivalence is reduced to 100 mm.

mm is less than that of a deep snowpack. In a similar manner, minute amounts of absorbing impurities reduce snow reflectance in the visible wavelengths (Warren and Wiscombe, 1980). Soot concentrations as low as 0.1 ppmw (parts per

million by weight) are enough to perceptibly reduce reflectance. The effect of the absorbing impurities is apparently enhanced when they are inside the snow grains, because refraction focuses the light on the absorbers (Grenfell et al., 1981; Chýlek et al., 1983; Bohren, 1986).

### Spectral Reflectance of Clouds and Snow/Cloud Discrimination

In visible satellite data, clouds can usually be distinguished from snow by texture, but not when both snow and clouds saturate the sensor, as might be the case in the spring. Moreover, in a computer image-processing system, texture is more difficult to analyze than spectral information. Hence we seek wavelength bands where snow and clouds have different spectral signatures. Clouds may be either warmer or colder than the snow surface, so that one cannot reliably distinguish clouds from snow in the thermal wavelengths. Properties that cause clouds to have different spectral reflectance than snow are, in order of importance:

1. Cloud droplets or ice crystals are smaller than snow grains. Cloud droplets usually have size radii less than  $10\ \mu\text{m}$ ; crystals in cirrus clouds can be as large as  $40\ \mu\text{m}$ , but most of them are smaller. A smaller scattering element—droplet, crystal, or grain—is likely to absorb less radiation, but the difference is greatest at wavelengths where the medium is modestly absorptive.
2. Most clouds are composed of water droplets, even at temperatures below  $0^\circ\text{C}$ . At most wavelengths in the optical region, water and ice have similar refractive indices, but ice is slightly more absorptive from  $1.55$  to  $1.7\ \mu\text{m}$ . The difference in the size of the scatterers between clouds and snow, however, is more important than the difference in composition.
3. Snow on the ground is usually optically thicker than clouds. Therefore in the visible wavelengths snow is sometimes brighter, because some of the light incident on the cloud is transmitted through it. Thick clouds, however, are as bright as snow, so that they cannot be dependably distinguished in this wavelength region by a lower reflectance. Cirrus clouds are

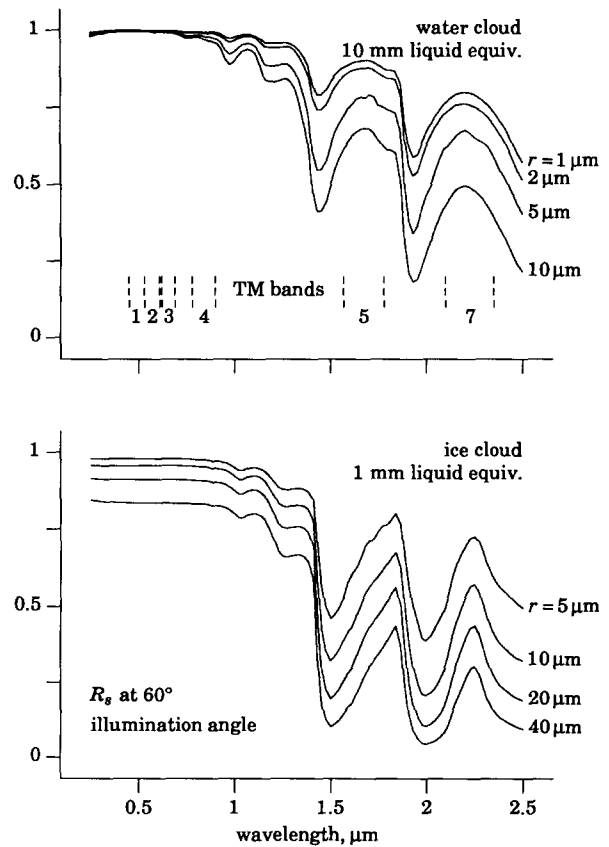


Figure 5. Directional-hemispherical reflectance  $R_s$  of water and ice clouds at illumination angle  $60^\circ$ , for wavelengths from  $0.4$  to  $2.5\ \mu\text{m}$ . Cloud liquid water equivalences are  $10\ \text{mm}$  for the water cloud and  $1\ \text{mm}$  for the ice cloud. Albedo of the underlying surface is set to  $0.3$  for both cases. The radii of the water droplets are, from top to bottom,  $1$ ,  $2$ ,  $5$ , and  $10\ \mu\text{m}$ . The radii of the ice crystals are, from top to bottom,  $5$ ,  $10$ ,  $20$ , and  $40\ \mu\text{m}$ . In the visible wavelengths ( $0.4$ – $0.7\ \mu\text{m}$ ) the ice clouds especially are less reflective than snow, because some of the light is transmitted through the cloud. In the near-infrared, reflectances of the clouds are greater than those of snow, especially from  $1.55$  to  $1.75\ \mu\text{m}$ .

usually thinner and have lower amounts of water per column of unit cross-sectional area.

Figure 5 shows spectral reflectances for water and ice clouds. The water clouds used in the calculation have a water-equivalent thickness of  $10\ \text{mm}$ , while the cirrus clouds have  $1\ \text{mm}$ . Therefore the water clouds are brighter. In the visible wavelengths the water clouds and the snowpack are of comparable reflectance. Plate II shows an example of snow/cloud discrimination in the southern Sierra Nevada, CA. In the left-hand image, TM Bands 1, 2, and 4, clouds can be discerned by their textural properties, but not their spectral charac-

teristics. Texture, unfortunately, is difficult to analyze in image processing. In the right-hand image, TM Bands 2, 4, and 5, clouds are clearly brighter than snow.

## MEASUREMENT OF SNOW PROPERTIES BY REMOTE SENSING

Satellite remote sensing in the visible and near-infrared wavelengths has become increasingly important to snow hydrologists because the data provide information on the spatial distribution of parameters of hydrologic importance. In snow and ice studies, remote sensing has been used to improve the monitoring of existing conditions and has been incorporated into several runoff forecasting and management systems. The principal operational use of remote sensing of snow properties has been to map the extent of the snow cover. Throughout the world, in both small and large basins, maps of the snow cover throughout the snow season are used to forecast melt, both in areas with excellent ancillary data and in remote areas with no ancillary data (Rango et al., 1977; Andersen, 1982; Martinec and Rango, 1986).

Since the first mapping of snow cover from satellite, the spectral and spatial resolution of the available sensors has been much improved. The high spatial resolution satellites such as Landsat and SPOT and the medium resolution sensors such as the NOAA AVHRR are widely used for mapping snow cover. The selection of the appropriate sensor depends on a tradeoff between spatial and temporal resolution (Rott, 1987). The Landsat Multispectral Scanning System (MSS) has a spatial resolution of about 80 m and is suitable for snow mapping in basins larger than about 10 km<sup>2</sup> (Rango et al., 1983). Improved spatial resolution has been available since 1982 from the Landsat Thematic Mapper (30 m) and since 1984 from the French SPOT satellite (20 m in the multispectral mode and 10 m in the panchromatic mode). SPOT has the finest spatial resolution, but the Thematic Mapper has the best spectral coverage.

### Incorporation of Topographic Effects in Atmospheric Radiation Model

In all but very gentle terrain, significant variation in remotely sensed images in visible and near-in-

frared wavelengths results from local topographic effects that cause variation in illumination angle and shadowing from local horizons (Williams et al., 1972; Dozier and Outcalt, 1979; Dozier et al., 1981a; Olyphant, 1984).

In the solar spectrum, irradiance in alpine terrain has three sources: 1)  $F_s$ , direct irradiance from the sun; 2)  $F_{\downarrow}^{(d)}$ , diffuse irradiance from the sky, where a portion of the overlying hemisphere is obscured by terrain; and 3)  $F_{\downarrow}^{(t)}$ , direct and diffuse irradiance, on nearby terrain, that is reflected toward the point whose radiation flux we want to calculate.

The direct irradiance on a slope is

$$F_s = \mu_s S_0 e^{-\tau_0/\mu_0}, \quad (10)$$

where  $\mu_s$  is the cosine of the local solar illumination angle on the slope.

Scattered diffuse irradiance from the sky is

$$F_{\downarrow}^{(d)} = V_d \overline{F_{\downarrow}}(\tau_0). \quad (11)$$

$\overline{F_{\downarrow}}$  is the mean downward irradiance on an unobstructed horizontal surface, obtained from the atmospheric transmittance. The sky-view factor  $V_d$  is the ratio of the diffuse sky irradiance at a point to that on an unobstructed horizontal surface, i.e.,  $0 < V_d \leq 1$ . It accounts for the slope and orientation of the point and the portion of the overlying hemisphere visible to the point. It can also be adapted to account for anisotropy in the diffuse irradiance, but the two-stream equations assume that diffuse irradiance is isotropic. Contribution from the surrounding terrain is

$$F_{\downarrow}^{(t)} = C_t \overline{F_{\uparrow}}(\tau_0). \quad (12)$$

The average radiation reflected from the surrounding terrain is  $\overline{F_{\uparrow}}$ . The terrain configuration factor  $C_t$  includes both the anisotropy of the radiation and the geometric effects between that point and each point in the surrounding terrain with which it is mutually visible. The contribution of each of these terrain elements to the configuration factor could be computed (Siegel and Howell, 1981), but this is a formidable computational problem. Rigorous calculation is difficult because it is necessary to consider every terrain facet visible from a point. In contrast to the sky radiation, the isotropic assumption is unrealistic because considerable anisotropy results from geometric effects even if the surrounding terrain is a Lambertian reflector.

We can now define an effective reflectance  $R_{\text{eff}}$ , the equivalent reflectance for a horizontal surface that would produce the same upwelling radiative flux  $F_{\uparrow}$  as the sloping surface, which has reflectance  $R_0$  and slope  $S$ :

$$R_{\text{eff}} = \frac{F_{\uparrow}(\tau_0)}{F_{\downarrow}(\tau_0) + \mu_0 S_0 e^{-\tau_0/\mu_0}} \quad (13a)$$

$$= R_0 \cos S \left[ V_d + C_t R_0 + \frac{e^{-\tau_0/\mu_0}}{T_s} \left( \frac{\mu_s}{\mu_0} - V_d \right) \right]. \quad (13b)$$

This value can now be used in place of  $R_0$  in Eq. (6) to calculate the planetary reflectance. Unfortunately, this detailed model of interaction between radiation and the terrain can only be used for simulation, because the quality of most digital elevation data is not good enough to calculate the slope and aspect of each pixel. Errors in the original elevation data are magnified by the differencing operations needed to compute the local gradient.

#### Automated Mapping of Snow Cover

The atmosphere/topography radiation model described in the previous sections is combined with calculations of the spectral reflectance of snow to simulate planetary reflectance for a range of snow grain sizes and topographic conditions. The atmosphere used in the simulations is the U.S. Standard with a rural background aerosol, 23 km surface visibility at sea level, and 50% relative humidity. The optical depths are adjusted to a surface pressure of 65–70 kPa. Table 3 lists the atmospheric optical properties in the reflective TM bands, and Table 4 lists the range of topographic variables.

The calculations show several ways in which snow can be distinguished from other surfaces and from clouds: Snow is brighter in TM Bands 1 and 2 than virtually all other surfaces. Although TM1

Table 3. Atmospheric Properties Used for Simulation

Band	$\tau_0$	$\omega_0$	$g$
TM1	0.4–0.6	0.93–0.97	0.44–0.50
TM2	0.25–0.35	0.87–0.92	0.50–0.55
TM3	0.2–0.3	0.87–0.92	0.55–0.58
TM4	0.15–0.25	0.75–0.85	0.61–0.63
TM5	0.1–0.15	0.55–0.65	0.66–0.68
TM7	0.05–0.1	0.4–0.6	0.66–0.68

Table 4. Terrain Characteristics of Sample Elevation Grid

Variable	Mean	Std Dev	Min	Max
Elevation (m)	3306	337	2182	4063
Slope (°)	30	15	0.2	68
$\mu_s$	0.41	0.29	0.0	0.98
$V_d$	0.85	0.10	0.35	1.00
$C_t$	0.07	0.06	0.00	0.34

saturates over most snow surfaces, it can be used to distinguish snow in shadowed areas. Clouds are brighter than snow in TM Band 5. These relationships suggest an automatic snow mapping procedure. All three of the following criteria must intersect for a pixel to be labeled as snow-covered.

1.  $R_p(\text{TM1})$  is greater than a threshold, which in the examples in this paper is about 0.16. Its precise value is not critical, but it usually lies between 0.15 and 0.2. This threshold distinguishes snow from other surfaces in shadowed areas. It will also apply to many surfaces that are not snow, but these are then rejected by one of the other criteria.
2.  $R_p(\text{TM5})$  is less than a threshold, which is about 0.2–0.25. This distinguishes snow from clouds.
3.  $[R_p(\text{TM2}) - R_p(\text{TM5})]/[R_p(\text{TM2}) + R_p(\text{TM5})]$  is greater than a threshold, which is about 0.4. This criterion, which rejects pixels whose reflectance in Band 5 is too great when compared to their reflectance in Band 2, helps distinguish snow from bright soils and rocks and from clouds.

The correct threshold values can be derived theoretically if the atmospheric properties at the time of the satellite overpass are known. More simply, however, one can select them by inspection of images, as the human eye can estimate the correct values by using textural features. Plate III shows this automated snow-mapping procedure. Pixels that meet each of the criteria are assigned separate primary colors; thus those pixels that are snow-covered and meet all three criteria are white in the image.

#### Estimation of Grain Size and Detection of Absorbing Impurities

In the visible wavelengths, we should be able to estimate the extent to which the reflectance of

snow has been degraded, either by absorbing impurities or by shallow depth. However, this sensitivity would be best for the blue wavelengths, where the low saturation values of the Thematic Mapper make its use for this purpose difficult. In the near-infrared wavelengths, we should be able to estimate the grain size, and thus extend the estimate of the spectral albedo throughout the solar wavelengths. Moreover, this information would help us interpret the spectral signature of snow at microwave frequencies.

Four indices would be useful to estimate grain size and contamination amount. Unfortunately, the first uses TM Band 1, which saturates over most snow-covered scenes.

1.  $[R_p(\text{TM1}) - R_p(\text{TM2})]/[R_p(\text{TM1}) + R_p(\text{TM2})]$  would serve as a contamination index if TM1 were not saturated. Higher values would represent cleaner snow.
2.  $[R_p(\text{TM2}) - R_p(\text{TM4})]/[R_p(\text{TM2}) + R_p(\text{TM4})]$  is a grain-size index for all sizes. Higher values represent larger grain sizes. It is also sensitive to contamination, but not enough to reliably estimate absorption by impurities.
3.  $[R_p(\text{TM2}) - R_p(\text{TM5})]/[R_p(\text{TM2}) + R_p(\text{TM5})]$  is also a grain-size index, and helps to identify the larger grains.
4.  $[R_p(\text{TM4}) - R_p(\text{TM5})]/[R_p(\text{TM4}) + R_p(\text{TM5})]$  is a grain-size index for finer grains. Higher values represent larger grain sizes.

Plates IV and V show my efforts to accomplish this interpretation, but the results are qualitative. Plate IV shows images of the southern Sierra Nevada in Bands 2, 4, and 5 for two dates in the winter of 1985: 25 February and 14 April. Plate V shows images made from the above indices that involve Bands 2, 4, and 5, processed to show only the snow-covered area, and to show the increases in grain size that occur during the season.

The largest sensitivity of snow reflectance to grain size occurs in the wavelengths from 1.0 to 1.3  $\mu\text{m}$ , beyond the range of Thematic Mapper Band 4 and below that of Band 5, which are currently not covered by any sensor. Future planned sensors with continuous spectral coverage, such as the High Resolution Imaging Spectrometer planned for the Earth Observing System (HIRIS Instrument Panel, 1987), should allow much more precise interpretation of the physical properties of surface snow.

## SUMMARY

Multispectral measurements in visible and near-infrared wavelengths have been used to map snow for more than two decades. Improved spectral coverage from the Landsat Thematic Mapper has allowed better estimation of snow properties and discrimination between snow cover and cloud cover. Future sensors with better spectral resolution should allow estimation of grain size and contamination by absorbing impurities, which in turn can be used to calculate spectral reflectance through the wavelengths of the solar spectrum.

## APPENDIX: NOTATION

- $d$  = Earth–Sun radius vector (mean = 1.0)
- $F$  = radiant flux ( $\text{W m}^{-2} \mu\text{m}^{-1}$ )
- $F_0$  = direct irradiance at top of medium ( $\text{W m}^{-2} \mu\text{m}^{-1}$ )
- $F_s$  = direct irradiance on slope ( $\text{W m}^{-2} \mu\text{m}^{-1}$ )
- $g$  = scattering asymmetry parameter
- $h$  = depth of snowpack (m)
- $k$  = imaginary part of index of refraction
- $L$  = radiant intensity ( $\text{W m}^{-2} \mu\text{m}^{-1} \text{sr}^{-1}$ )
- $n$  = real part of index of refraction
- $Q_{\text{cal}}$  = digital radiance number
- $R_0$  = surface reflectance (general)
- $R_{\text{eff}}$  = effective surface reflectance, accounting for topography
- $R_p$  = apparent planetary reflectance
- $R_s$  = directional-hemispherical reflectance
- $r$  = equivalent spherical radius of scatterer
- $S$  = slope angle
- $S_0$  = exoatmospheric solar irradiance ( $\text{W m}^{-2} \mu\text{m}^{-1}$ )
- $W$  = snow water equivalence ( $\text{kg m}^{-2}$ ); note that 1 mm water =  $1 \text{ kg m}^{-2}$
- $\gamma$  = parameters to describe angular distribution of scattering phase function
- $\lambda$  = wavelength ( $\mu\text{m}$ )
- $\mu$  = cosine of angle measured from normal
- $\mu_0$  = cosine of illumination angle on horizontal surface
- $\mu_s$  = cosine of local illumination angle on slope
- $\rho$  = density ( $\text{kg m}^{-3}$ )
- $\tau$  = optical depth coordinate
- $\tau_0$  = optical depth of atmosphere
- $\omega_0$  = single scattering albedo

The simplifying variables  $P^\pm$ ,  $q$ ,  $Q^\pm$ ,  $U^\pm$ ,  $V^\pm$ ,  $\xi$ ,  $\alpha_1$ , and  $\alpha_2$  are defined following Eq. (7).

*This work was supported by the National Aeronautics and Space Administration under Grant AS 5-28770. I am indebted to Warren Wiscombe for his Mie scattering codes.*

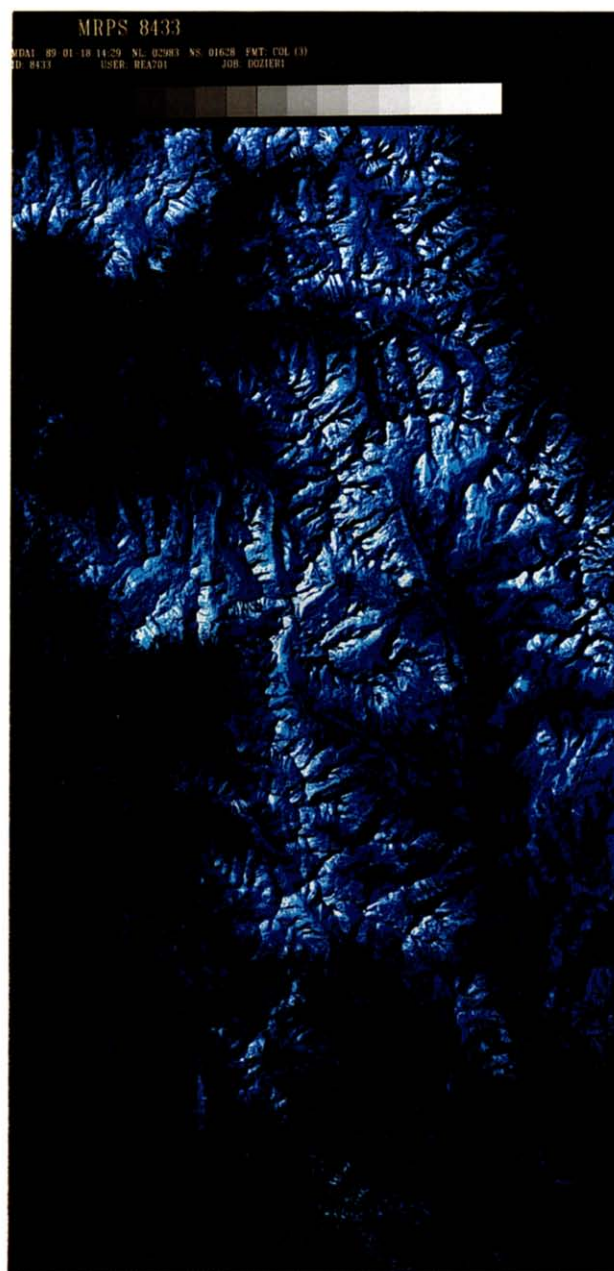
## REFERENCES

- Andersen, T. (1982), Operational snow mapping by satellites, in *Hydrological Aspects of Alpine and High-Mountain Areas* (J. W. Glen, Ed.), IAHS Publ. No. 138, Intl. Assoc. Hydrol. Sci., Wallingford, UK, pp. 149–154.
- Barker, J. L., and Wanchoo, L. (1989), Radiometric performance of the Landsat Thematic Mappers, *Remote Sens. Environ.* (this issue).
- Bohren, C. F. (1986), Applicability of effective-medium theories to problems of scattering and absorption by nonhomogeneous atmospheric particles, *J. Atmos. Sci.* 43:468–475.
- Bohren, C. F., and Barkstrom, B. R. (1974), Theory of the optical properties of snow, *J. Geophys. Res.* 79:4527–4535.
- Chandrasekhar, S. (1960), *Radiative Transfer*, Dover, New York, 393 pp.
- Chýlek, P., Ramaswamy, V., and Srivastava, V. (1983), Albedo of soot-contaminated snow, *J. Geophys. Res.* 88:10,837–10,843.
- Colbeck, S. C. (1979), Grain clusters in wet snow, *J. Colloid Interface Sci.* 72:371–384.
- Colbeck, S. C. (1986), Classification of seasonal snow cover crystals, *Water Resour. Res.* 22:59S–70S.
- Colbeck, S. C., Anderson, E. A., Bissel, V. C., Crook, A. G., Male, D. H., Slaughter, C. W., and Wiesnet, D. R. (1979), Snow accumulation, distribution, melt, and runoff, *EOS, Trans. Am. Geophys. Union* 60:465–474.
- Crane, R. G., and Anderson, M. R. (1984), Satellite discrimination of snow/cloud surfaces, *Int. J. Remote Sens.* 5:213–223.
- Davis, R. E., and Dozier, J. (1989), Stereological characterization of dry alpine snow for microwave remote sensing, *Adv. Space Res.*, forthcoming.
- Downing, H., and Williams, D. (1975), Optical constants of water in the infrared, *J. Geophys. Res.* 80:1656–1661.
- Dozier, J. (1984), Snow reflectance from Landsat-4 Thematic Mapper, *IEEE Trans. Geosci. Remote Sens.* GE-22:323–328.
- Dozier, J., and Outcalt, S. I. (1979), An approach toward energy balance simulation over rugged terrain, *Geogr. Anal.* 11:65–85.
- Dozier, J., Bruno, J., and Downey, P. (1981a), A faster solution to the horizon problem, *Comput. Geosci.* 7:145–151.
- Dozier, J., Schneider, S. R., and McGinnis, D. F., Jr. (1981b), Effect of grain size and snowpack water equivalence on visible and near-infrared satellite observations of snow, *Water Resour. Res.* 17:1213–1221.
- Dozier, J., Davis, R. E., Chang, A. T. C., and Brown, K. (1988), The spectral bidirectional reflectance of snow, in *Spectral Signatures of Objects in Remote Sensing*, Fourth Int. Colloq., ESA SP-287, European Space Agency, Paris, pp. 87–92.
- Grenfell, T. C., Perovich, D. K., and Ogren, J. A. (1981), Spectral albedoes of an alpine snowpack, *Cold Regions Sci. Technol.* 4:121–127.
- Hale, G. M., and Querry, M. R. (1973), Optical constants of water in the 200-nm to 200- $\mu$ m wavelength region, *Appl. Opt.* 12:555–563.
- HIRIS Instrument Panel (1987), *HIRIS—High-Resolution Imaging Spectrometry: Science Opportunities for the 1990s*, Earth Obs. Sys. Rep. 2c, NASA, Washington, DC, 74 pp.
- Hyvärinen, T., and Lammasniemi, J. (1987), Infrared measurement of free-water content and grain size of snow, *Opt. Eng.* 26:342–348.
- Kneizys, F. X., Shettle, E. P., Gallery, W. O., Jr., J. H. Chetwynd, Abreu, L. W., Selby, J. E. A., Clough, S. A., and Fenn, R. W. (1983), Atmospheric transmittance/radiance: computer code LOWTRAN6, Rep. AFGL-TR-83-0187, Air Force Geophys. Lab., Bedford, MA.
- Markham, B. L., and Barker, J. L. (1985), Spectral characterization of the Landsat Thematic Mapper sensors, *Int. J. Remote Sens.* 6:697–716.
- Markham, B. L., and Barker, J. L. (1987), Thematic Mapper bandpass solar exoatmospheric irradiances, *Int. J. Remote Sens.* 8:517–523.
- Martinec, J., and Rango, A. (1986), Parameter values for snowmelt runoff modelling, *J. Hydrol.* 84:197–219.
- Meador, W. E., and Weaver, W. R. (1980), Two-stream approximations to radiative transfer in planetary atmospheres: a unified description of existing methods and a new improvement, *J. Atmos. Sci.* 37:630–643.
- Meier, M. F. (1984), Contribution of small glaciers to global sea level, *Science* 226:1418–1421.
- Nicodemus, F. E., Richmond, J. C., Hsia, J. J., Ginsberg, I. W., and Limperis, T. (1977), *Geometrical Considerations and Nomenclature for Reflectance*, Natl. Bur. Stds. Monogr. 160, U.S. Dept. of Commerce, Washington, DC, 52 pp.
- Nussenzweig, H. M., and Wiscombe, W. J. (1980), Efficiency factors in Mie scattering, *Phys. Rev. Lett.* 45:1490–1494.
- Olyphant, G. A. (1984), Insolation topoclimates and potential ablation in alpine snow accumulation basins: Front Range, Colorado, *Water Resour. Res.* 20:491–498.
- Palmer, K. and Williams, D. (1974), Optical properties of water in the near infrared, *J. Opt. Soc. Am.* 64:1107–1110.
- Rango, A., and Itten, K. I. (1976), Satellite potentials in snowcover monitoring and runoff prediction, *Nordic Hydrol.* 7:209–230.

- Rango, A., and Martinec, J. (1979), Application of a snowmelt-runoff model using Landsat data, *Nordic Hydrol.* 10:225–238.
- Rango, A., Salomonson, V. V., and Foster, J. L. (1977), Seasonal streamflow estimation in the Himalayan region employing meteorological satellite snow cover observations, *Water Resour. Res.* 14:359–373.
- Rango, A., Martinec, J., Foster, J., and Marks, D. (1983), Resolution in operational remote sensing of snow cover, in *Hydrological Applications of Remote Sensing and Remote Data Transmission* (B. E. Goodison, Ed.), IAHS Publ. No. 145, Int. Assoc. Hydrol. Sci., Wallingford, UK, pp. 371–382.
- Rott, H. (1987), Remote sensing of snow, in *Large Scale Effects of Seasonal Snow Cover* (B. E. Goodison, R. G. Barry, and J. Dozier, Eds.), IAHS Publ. No. 166, Int. Assoc. Hydrol. Sci., Wallingford, UK, pp. 279–290.
- Siegel, R., and Howell, J. R. (1981), *Thermal Radiation Heat Transfer*, 2nd ed., McGraw-Hill, New York, 862 pp.
- Valovcin, F. R. (1976), Snow/cloud discrimination, Rep. AFGL-TR-76-0174, Air Force Geophys. Lab., Hanscom Air Force Base, MA.
- Walsh, J. E. (1984), Snow cover and atmospheric variability, *Am. Sci.* 72:50–57.
- Warren, S. G. (1982), Optical properties of snow, *Rev. Geophys. Space Phys.* 20:67–89.
- Warren, S. G. (1984), Optical constants of ice from the ultraviolet to the microwave, *Appl. Opt.* 23:1206–1225.
- Warren, S. G., and Wiscombe, W. J. (1980), A model for the spectral albedo of snow, II, Snow containing atmospheric aerosols, *J. Atmos. Sci.* 37:2734–2745.
- Williams, L. D., Barry, R. G., and Andrews, J. T. (1972), Application of computed global radiation for areas of high relief, *J. Appl. Meteorol.* 11:526–533.
- Wiscombe, W. J., and Warren, S. G. (1980), A model for the spectral albedo of snow, I, Pure snow, *J. Atmos. Sci.* 37:2712–2733.



*Plate 1.* Saturated pixels in TM Bands 1, 2, and 4 for image of southern Sierra Nevada on 25 February 1985. Dimensions in this and all other images are  $85 \times 47 \text{ km}^2$ . The left image shows TM Bands 1 (blue), 2 (green), and 4 (red). In the right



image, pixels are colored blue if they are saturated in TM1, green in TM2, and red in TM4. Thus pixels that are saturated in all three bands are white, and the cyan pixels are saturated in TM1 and TM2. Pixels saturated in only TM2 and TM4 would be yellow, and those saturated in only TM1 and TM4 would be magenta, but these combinations do not occur.

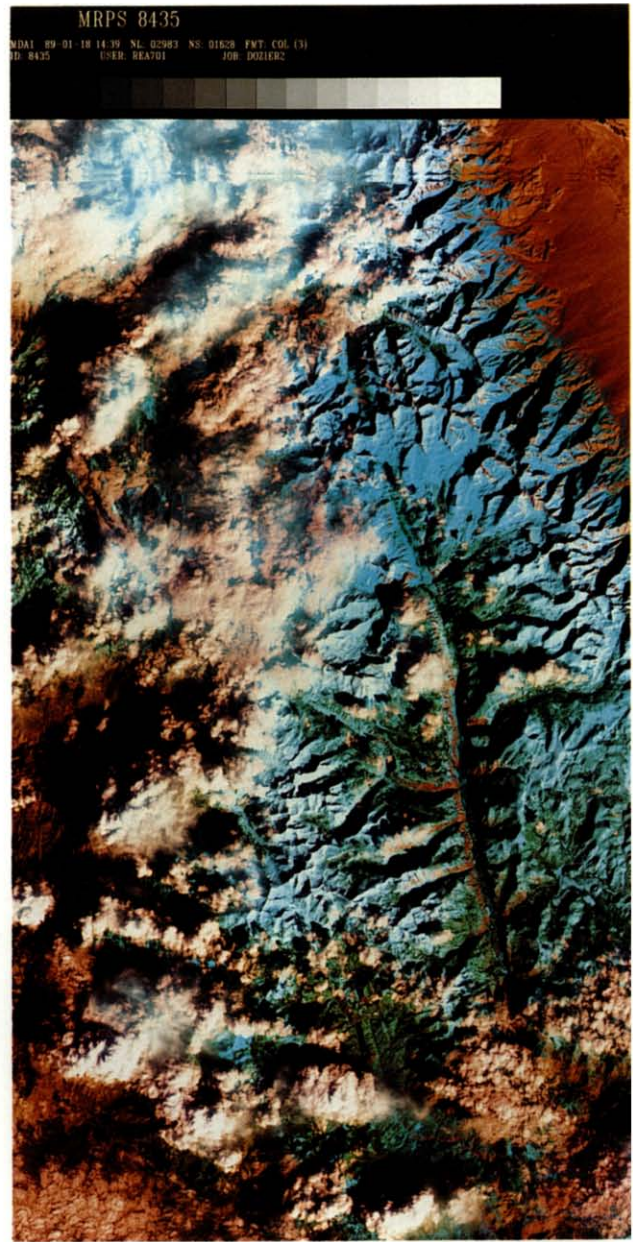


*Plate II.* Snow/cloud discrimination from the Landsat Thematic Mapper, for the southern Sierra Nevada, 24 January 1985. North is to the top. The left photograph is made from TM Bands 1, 2, and 4, the right from TM Bands 2, 4, and 5.

Although clouds can be texturally distinguished from snow in the left image, the right image, which includes TM5 spectrally discriminates clouds from snow.

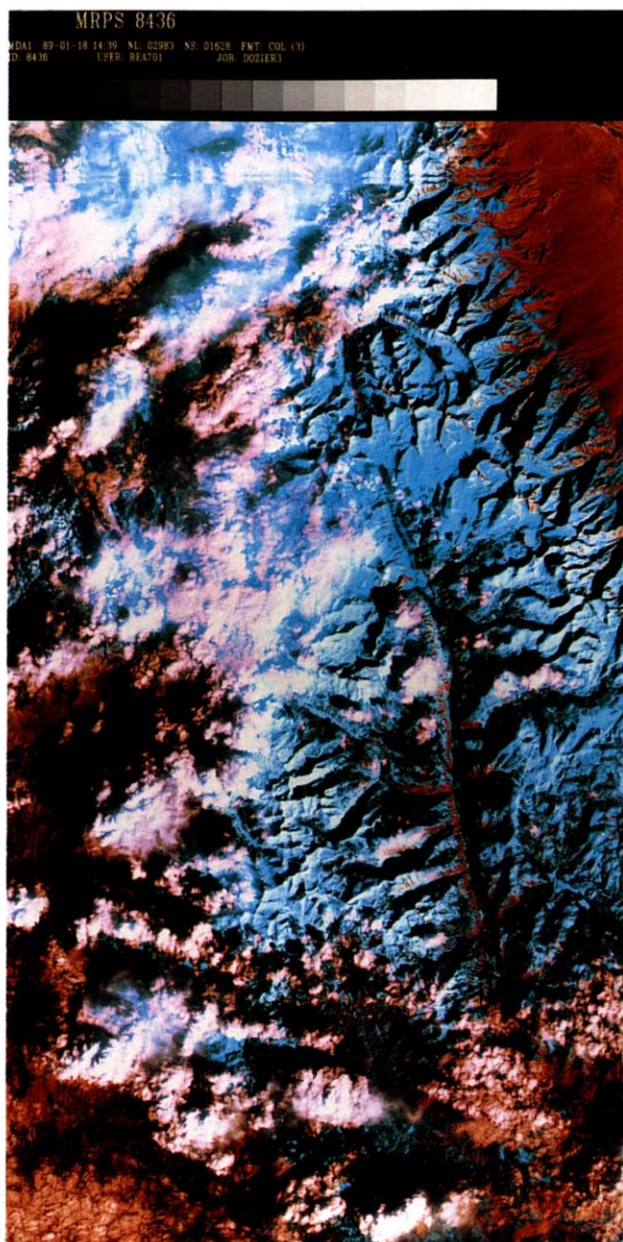


*Plate III.* Automated mapping of snow cover from TM Bands 1, 2, and 5, for the southern Sierra Nevada, 24 January 1985. The left image shows TM Bands 1 (blue), 2 (green), and 5 (red). The right image shows the following color codes: blue—bright enough in band 1 to be snow; red—dark enough in

Band 5; green—Band 2-5 index high enough. Thus white, snow-covered pixels are those that pass all three criteria. Black pixels passed none of the criteria, and colored pixels passed one or two of them.

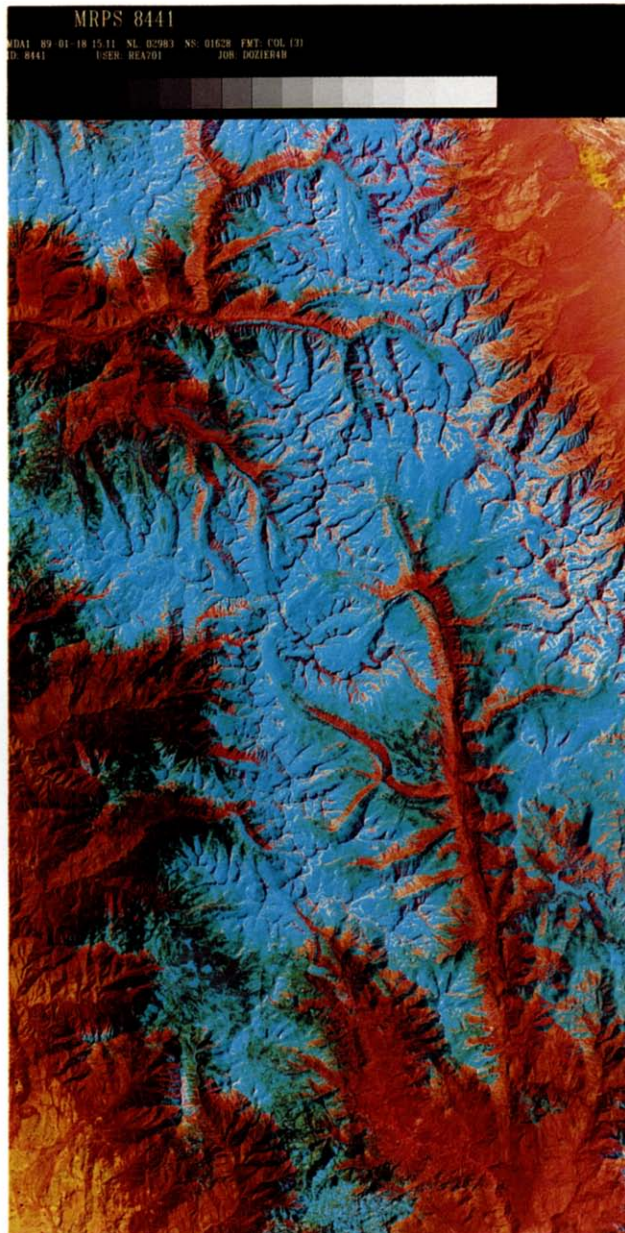


*Plate IV.* TM images of the southern Sierra Nevada on 25 February and 14 April, 1985, with Band 2 in blue, 4 in green, and 5 in red. These are analyzed for grain size in Plate V.

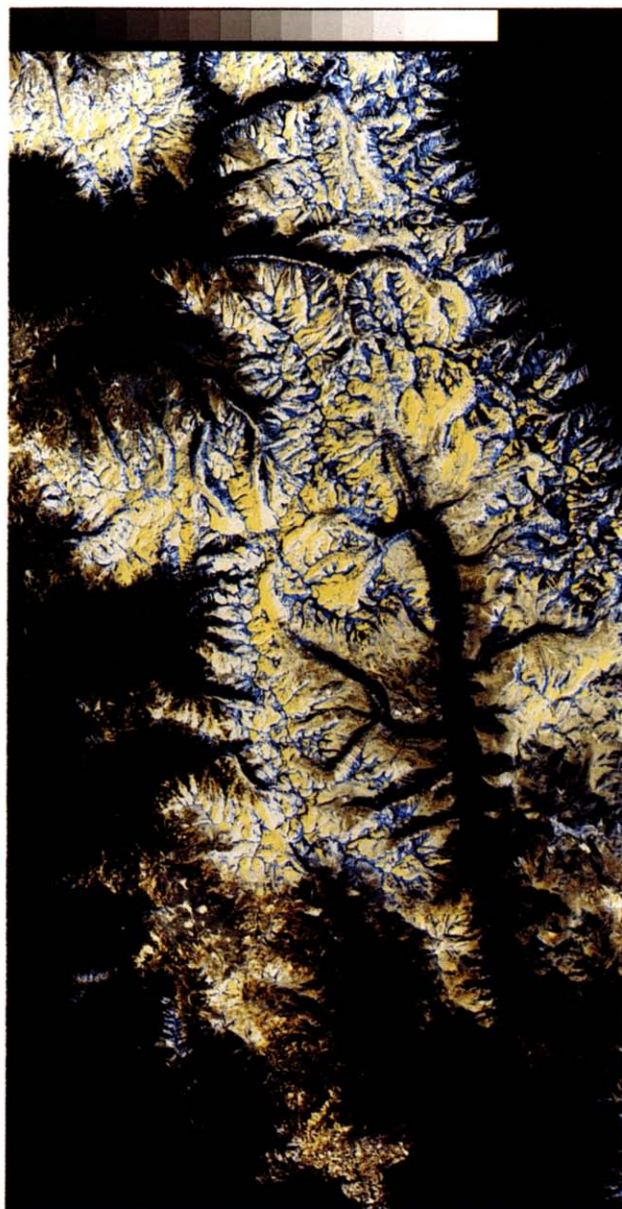


*Plate V.* Snow properties from Landsat TM band 4 in the southern Sierra Nevada in 1985: 25 February (left) and 14 April (right). These have been processed to show variations in grain size for the snow-covered area. The Band 2-4 index is

blue, the 2-5 index is green, and the 4-5 index is red. Thus the white or faint blue pixels represent the finest grains, blue larger grains, yellow or orange larger still, and red or brown the largest grains.